J Appl Electrochem (2010) 40:675–681
DOI 10.1007/s10800-009-0042-9

ORIGINAL PAPER

Structural optimization of gas diffusion electrodes loaded with $LaMnO_3$ electrocatalysts

Masayoshi Yuasa · Akiko Koga · Tetsuya Kida · Kengo Shimanoe · Noboru Yamazoe

Received: 2 July 2009 / Accepted: 23 November 2009 / Published online: 11 December 2009

Abstract In this study, gas diffusion electrodes (GDEs) with two catalyst layers were fabricated and tested for their electrode performance for oxygen reduction in an alkaline solution. The $LaMnO_3$/carbon black catalyst layers were fabricated using a reverse micelle method to finely disperse the $LaMnO_3$ particles onto the carbon matrices, for which commercial Ketjen Black (KB) (1270 $m^2\ g^{-1}$) and Vulcan XC-72R (VX) (254 $m^2\ g^{-1}$) were used. The three-layer-structured GDE with the two $LaMnO_3$/KB and $LaMnO_3$/VX catalyst layers exhibited a superior oxygen reduction activity when compared to that of a conventional GDE with only one $LaMnO_3$/KB catalyst layer. Pore size distribution and gas permeability measurements revealed that the $LaMnO_3$/VX layer was more porous and had higher gas permeability than the $LaMnO_3$/KB layer. These results suggest that the intermediate layer of $LaMnO_3$/VX can efficiently supply oxygen to reaction sites dispersed in the $LaMnO_3$/KB and $LaMnO_3$/VX catalyst layers, which consequently leads to an improvement in the electrode performance.

Keywords Gas diffusion electrode · Oxygen reduction · Pt-free catalyst · Brine electrolysis

M. Yuasa (✉) · T. Kida · K. Shimanoe · N. Yamazoe
Department of Energy and Material Sciences, Faculty of Engineering Sciences, Kyushu University, 6-1 Kasuga Koen, Kasuga-shi, Fukuoka 816-8580, Japan
e-mail: yuasa@mm.kyushu-u.ac.jp

A. Koga
Department of Energy Science and Engineering, Kyushu University, 6-1 Kasuga Koen, Kasuga-shi, Fukuoka 816-8580, Japan

1 Introduction

Gas diffusion-type oxygen reduction electrodes (GDEs) have been intensively investigated for various applications, including metal-air batteries [1, 2], brine electrolysis [3, 4], fuel cell [5], and electrogeneration processes [6]. Typically, electrodes of this type are composed of two layers, i.e., a gas diffusion layer and a catalyst layer, as is schematically shown in Fig. 1a. The gas diffusion layer is made from hydrophobic carbon black, mixed with polytetrafluoroethylene (Teflon® PTFE). This layer has a porous structure to supply oxygen to the catalyst layer, and its hydrophobic nature prevents leakage of aqueous electrolytes. Conversely, the catalyst layer is made from catalyst-loaded hydrophilic carbon black, mixed with PTFE. At the hydrophilic catalyst layer, which is in contact with an electrolyte, oxygen supplied through the hydrophobic gas diffusion layer is reduced to form hydroxide ions. It has been shown that the oxygen reduction reaction on carbon black occurs via a two-electron reaction pathway to generate hydrogen peroxide, which corrodes the carbon support to form carbon monoxide (CO) or water-soluble organic compounds [7]. However, a noble metal or metal oxide electrocatalyst can reduce oxygen to hydroxide via a four-electron reaction pathway, suppressing the corrosion of the carbon supports. Therefore, the loading of the electrocatalysts on the carbon supports is indispensable for GDEs in terms of the oxygen reduction efficiency and electrode stability. Among the electrocatalysts investigated so far, noble metals such as Pt (or Pt-based alloys) [8–14] and Ag [15–17] were found to show the highest activity for oxygen reduction. Indeed, Pt-loaded carbon electrodes have been used as air electrodes for commercial metal-air batteries and electrodes for fuel cells. However, the

increasing price of noble metals restricts their extensive commercial use, and thus low-cost electrocatalysts have been in great demand. This motivated many researchers to concentrate their studies on single- or mixed-transition metal oxide-based electrocatalysts [18–24]. Meadowcroft was the first to show the potential of perovskite-type oxides to be used as electrocatalysts for oxygen reduction electrodes [25]. In his report, the electrocatalytic properties of perovskite-type oxides have been intensively studied.

We have reported that lanthanum manganite-based ABO_3 perovskites (with A- and B-sites partially substituted such as $La_{1-x}Sr_xMn_{1-y}Fe_yO_3$ and $La_{1-x}Ca_xMn_{1-y}Fe_yO_3$) are promising, in view of both their electro-catalytic activity and stability [26]. Conventionally, the perovskite-type oxides are synthesized by high temperature calcination and then mechanically mixed with carbon powder, to prepare the carbon-supported electrocatalysts. However, this route normally produces large aggregated particles with low surface areas, and it is difficult to homogeneously disperse the particles onto the carbon supports. It is well known that the high dispersion of electrocatalysts with high surface areas onto carbon supports usually leads to an increase in the electrocatalytic activity. Hence, to achieve homogeneous deposition of perovskite oxides on carbon supports and thus to give high electrocatalytic activity, we focused on a reverse micelle (RM) method for the fabrication of a catalyst layer for GDEs [27–31]. In this method, nano-sized precursor hydroxides are prepared inside nano-sized water droplets (reverse micelles), surrounded by surfactants, in an organic solvent. Since carbon black is readily dispersed in an organic phase, the addition of carbon black (support) into the reverse micelle solution results in homogeneous deposition of the precursor hydroxides onto the carbon black. The obtained hydroxide deposited on the carbon black was calcined under a nitrogen flow to form the perovskite-type oxide. By using $La_{1-x}Sr_xMn_{1-y}Fe_yO_3$-loaded carbon electrodes, fabricated through the RM method, we achieved relatively small overpotentials for oxygen reduction [32], which are similar to those for Pt-loaded carbon electrodes.

In addition to the dispersion state of the electrocatalysts in the catalyst layer, the macro- and micro-structures of the catalyst layer are also important for improving the activity of GDEs. As mentioned above, oxygen diffusing through the gas diffusion layer is reduced at the catalyst layer, and thus the electrode activity is also dependent on the diffusion rate of oxygen. Thus, the structural optimization of GDEs, in which the hydrophobic gas diffusion and hydrophilic catalyst layers are stacked, is important to improve the oxygen diffusion and reduction rates. In this study, a new electrode structure, in which a porous hydrophilic catalyst layer is inserted between the gas diffusion and catalyst layers, was designed, as is schematically shown in Fig. 1b. The three-layer-structure of the GDEs was expected to assist in the oxygen diffusion. Another important feature of the three-layer-structure is that the electrode thickness can be adjusted. It is expected that an increase in electrode thickness will bring about an improvement in the oxygen reduction activity, because of an increase in the number of active sites. Under these conditions, it is anticipated that oxygen will efficiently diffuse through the whole catalyst layer. Furthermore, an increase in the thickness of GDEs may be expected to improve their durability during long-term operation. GDEs of 1–2 mm in thickness are stable and are used, in practice, as prototypes for energy saving-type brine electrolysis. Here, we report the oxygen reduction properties of the three-layer-structured GDEs loaded with $LaMnO_3$ electrocatalysts prepared through the RM method, and discuss the performance in terms of thickness, pore size distribution, and gas permeability of the catalyst layers.

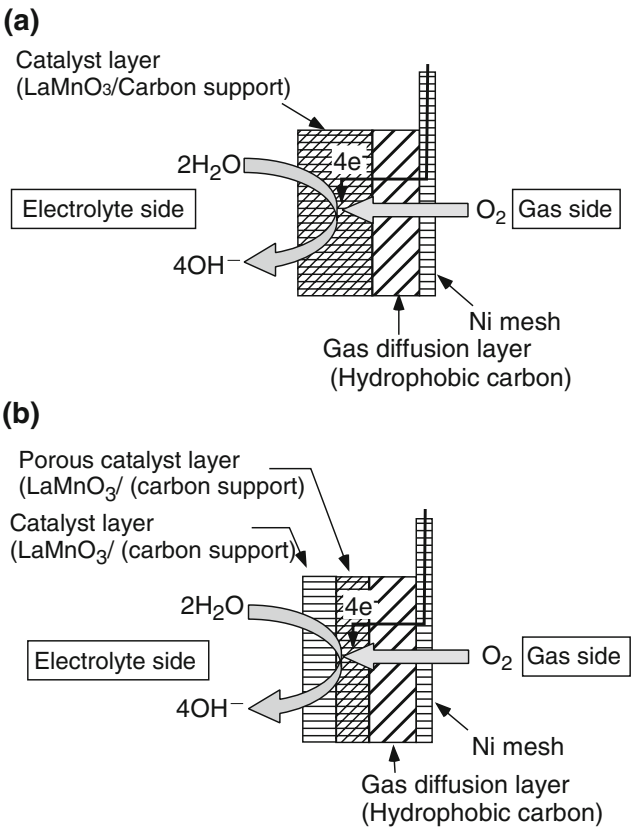

Fig. 1 Schematic drawing of gas diffusion electrodes (GDEs). **a** conventional type, **b** three-layer-structure type (proposed in this study)

2 Experimental

2.1 Preparation of $LaMnO_3$-loaded carbon using the RM method

Figure 2 shows the preparation procedure for $LaMnO_3$-loaded carbon black using an RM method. By adopting the RM method, nano-sized $LaMnO_3$ can be finely loaded onto carbon matrices as previously reported [28–30]. Initially, two reverse micelle solutions, denoted as RM-A and RM-B, were prepared, respectively, by adding aqueous solutions containing La and Mn nitrates (0.2 mol l^{-1}) and tetramethylammonium hydroxide (TMAH; 10 wt%) separately into organic solutions containing cyclohexane and nonionic surfactant (hexaethylene glycol nonylphenyl ether; NP-6). The volume ratio of the solutions containing the La and Mn nitrates to the TMAH solution and the molar ratio of surfactant to each aqueous solution were set to 3 and 9, respectively. The two reverse micelle solutions were vigorously stirred at 10 °C for 0.5–2 h until the solutions became transparent. Then, the two reverse micelle solutions were mixed together at 10 °C and stirred for 2 h, resulting in the formation of a dark-brown colored dispersion containing precursor hydroxide particles. The final dispersion obtained is hereafter denoted as RM-C.

Two typical carbon supports, commercial Ketjen Black (KB) (Ketjen Black International Co., specific surface area: 1270 m^2 g^{-1}, hydrophilic) and Vulcan XC-72R (VX) (Cabot Co., specific surface area; 254 m^2 g^{-1}, hydrophilic) were used. Carbon black was dispersed in cyclohexane under ultrasonic agitation (45 kHz) for 10 min to attain a homogeneous dispersion. The carbon black dispersion was added into the RM-C solution, to deposit the precursor hydroxide particles onto the carbon black. The weight ratio of the precursor hydroxide to carbon was fixed at 30:70. The reverse micelles were broken up by adding ethanol into the dispersion, and then the hydroxides were deposited onto the carbon black. By allowing the solution to stand, the hydroxide-deposited carbon black was subsequently precipitated. The precipitates were collected and washed by filtration using ethanol. The collected particles were calcined at 650 °C for 5 h under a N_2 flow to obtain $LaMnO_3$-loaded carbon (KB or VX).

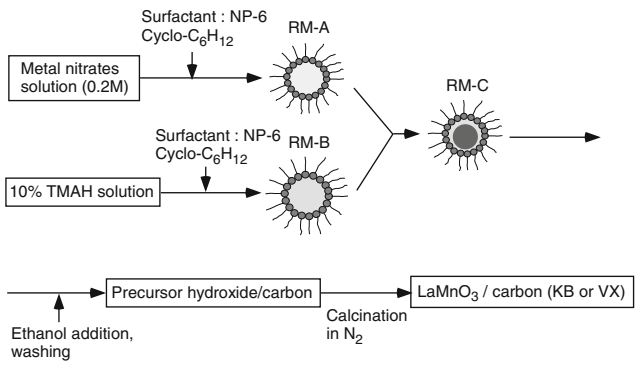

Fig. 2 Preparation scheme of $LaMnO_3$-loaded carbon by the reverse micelle method

2.2 Fabrication of GDEs

GDEs with two catalyst layers were fabricated as schematically shown in Fig. 1b. The catalyst layers were composed of the $LaMnO_3$-loaded KB or VX carbon black prepared above. For comparison, GDEs with conventional structures, as shown in Fig. 1a, were also fabricated. In this case, the catalyst layer was composed of $LaMnO_3$-loaded KB carbon black.

The fabrication procedures for the GDEs were as follows. The $LaMnO_3$-loaded carbon black, prepared above, was dispersed in deionized water, and then mixed with a PTFE dispersion (Daikin Industries, Ltd.) together with a small amount of n-butanol, under vigorous stirring. PTFE acts as a binder between the $LaMnO_3$-loaded carbon black particles. The mixture was then filtered, and the resulting precipitates were dried at 120 °C. The weight ratio of the $LaMnO_3$-loaded carbon to PTFE was fixed at 85:15. The powder obtained, was used for fabricating the catalyst layers. The powder for the gas diffusion layers was prepared using the following procedure. Acetylene black carbon powder (AB-7; Denki Kagaku, Inc., Co., specific surface area: 47 m^2 g^{-1}, hydrophobic), PTFE, and Triton-X were mixed in deionized water. Triton-X was used as a dispersing agent for AB-7 because AB-7 is difficult to disperse in water, due to its hydrophobic nature. The weight ratio of AB-7 to PTFE was set to 7:3. After filtration and drying at 120 °C, the mixed powder was then heat-treated at 280 °C in air to remove the Triton-X from the powder.

Gas diffusion electrodes 7 mm in diameter (1.54 cm^2 in geometric surface area) and 0.4 mm in thickness were fabricated by stacking a gas diffusion layer (0.2 mm thickness) and catalyst layers (0.24–0.92 mm thickness) on a Ni mesh current collector (100 mesh, Nilaco. Co., Ltd), using the following procedure. Initially, the powdered mixture of AB-7 and PTFE was spread over the Ni mesh and compressed at 1.6 MPa to form the gas diffusion layer. The $LaMnO_3$/carbon powder mixed with PTFE was then spread over the top of this layer and compressed at 3.2 MPa to form the catalyst layer. For the fabrication of the GDEs with the two catalyst layers, a second catalyst layer was also stacked on the top layer using the same procedure. Finally, the gas diffusion layer and catalyst layers stacked onto the Ni mesh were heat-compressed at 360 °C at 6.4 MPa.

Table 1 Structure and thickness of the electrodes fabricated in this study

Layer structure	Electrode	Component of the catalyst layer	Thickness of the catalyst layer		
			Electrolyte side layer (μm)	Intermediate layer (μm)	Total (μm)
Two layers	A	$LaMnO_3$/Ketjen Black			240
	B				540
	C				920
	F	$LaMnO_3$/Vulcan XC-72			340
Three layers	D	Intermediate layer: $LaMnO_3$/Vulcan XC-72	170	170	340
		Electrolyte side layer: $LaMnO_3$/Ketjen Black			
	D′	Intermediate layer: Vulcan XC-72	170	170	340
		Electrolyte side layer: $LaMnO_3$/Ketjen Black			
	D″	Intermediate layer: $LaMnO_3$/Vulcan XC-72	170	170	340
		Electrolyte side layer: Ketjen Black			
	E	Intermediate layer: $LaMnO_3$/Ketjen Black	170	170	340
		Electrolyte side layer: $LaMnO_3$/Vulcan XC-72			
	G	Intermediate layer: $LaMnO_3$/Vulcan XC-72	270	270	540
		Electrolyte side layer: $LaMnO_3$/Ketjen Black			

Table 1 summarizes the type and thickness of catalyst layers of the fabricated GDEs, which are referred to as Electrodes A, B, C, D, D′, D″, E, F, and G. Electrodes A, B, and C are conventional types with different thicknesses; all their catalyst layers are composed of $LaMnO_3$/KB. For Electrode F (conventional type), the catalyst layer was replaced with a $LaMnO_3$/VX layer. Electrodes D, D′, D″, E, and G are three-layer-structured electrodes with two catalyst layers; their catalyst layers were made of $LaMnO_3$/KB or $LaMnO_3$/VX. The thickness of each catalyst layer was 170 mm, for Electrodes D through to F. For Electrode G, the thickness of each catalyst layer was 270 mm. The stacking orders of the two catalyst layers for the three-layer-structured GDEs are shown in Table 1. For Electrodes D′ and D″, the $LaMnO_3$ catalyst was removed from one of the two layers.

2.3 Characterization of fabricated electrodes and evaluation of their oxygen reduction activity

The surface area of $LaMnO_3$/carbon powders was measured by the Brunauer, Emmet, Teller (BET) method using gas adsorption instrumentation (BELSORP-mini, BEL Japan, Inc.). The pore size distribution of the catalyst and gas diffusion layers was measured using a mercury porosimeter (PoreSizer 9320; Shimadzu Co., Ltd.). The gas permeability of the catalyst layers was evaluated by measuring their nitrogen permeation rates, at room temperature. For the measurements, a pressure difference was applied across the layer, with the low-pressure side of the layer being kept at atmospheric pressure. The nitrogen permeation rate was then measured using a flow meter.

The fabricated GDE was mounted in a Teflon cell and the nickel side of the electrode was connected to the working electrode terminal of a potentiostat (HA-305, Hokuto Denko, Co., Ltd.) using a Cu wire. NaOH (9 mol L^{-1}) solution, at 80 °C, was poured into the Teflon cell to act as an electrolyte. A Pt plate and a Hg/HgO electrode were used as the counter and reference electrodes, respectively. Polarization curves were measured by using the potentiostat, under an O_2 flow (100 cm^3 min^{-1}).

3 Results and discussions

3.1 Effect of electrode thickness on oxygen reduction properties

The effect of electrode thickness on the oxygen reduction activity for the conventional-type GDEs was initially investigated. Figure 3a shows the polarization curves of the three conventional electrodes (Electrodes A, B, and C mentioned in Table 1) with different $LaMnO_3$/KB catalyst layer thicknesses. At a current density of less than 300 mA cm^{-2}, the overpotentials for oxygen reduction decreased with increasing the thickness of the electrodes from 240 to 540 μm. This is presumably because of an increase in the number of reaction sites for oxygen reduction. However, at a current density higher than 300 mA/cm^2, the overpotentials increased with increasing the electrode thickness from 240 to 920 μm. In particular, at around 500 mA cm^{-2}, the overpotential increased sharply for the thick electrodes. This tendency was more conspicuous when air was introduced in place of the

oxygen, although the data obtained are not shown here. In order to more clearly show the effect of oxygen supply to reaction sites on the electrode performance, polarization curves were replotted according to the Tafel equation (E-logI plot), as shown in Fig. 3b. It is known that an E-logI plot, when electrode reactions are not mass transport limited, yields a straight line obeying the Tafel equation. From comparison of the dotted lines and solid lines in Fig. 3b, it follows that the deviation from the Tafel equation becomes larger with increasing the thickness of the catalyst layer from 240 to 920 μm. This suggests that as the thickness of the GDEs increases, oxygen supply through the catalyst layer, to the reaction sites in contact with the electrolyte, becomes insufficient for oxygen reduction to proceed efficiently at the high current density region. Hence, the porosity and gas permeability of the catalyst layer should also be taken into consideration when increasing the thickness of GDEs. In the next section, the structure of the catalyst layer was controlled using $LaMnO_3$/KB and $LaMnO_3$/VX with different surface areas, porosities, and gas permeabilities.

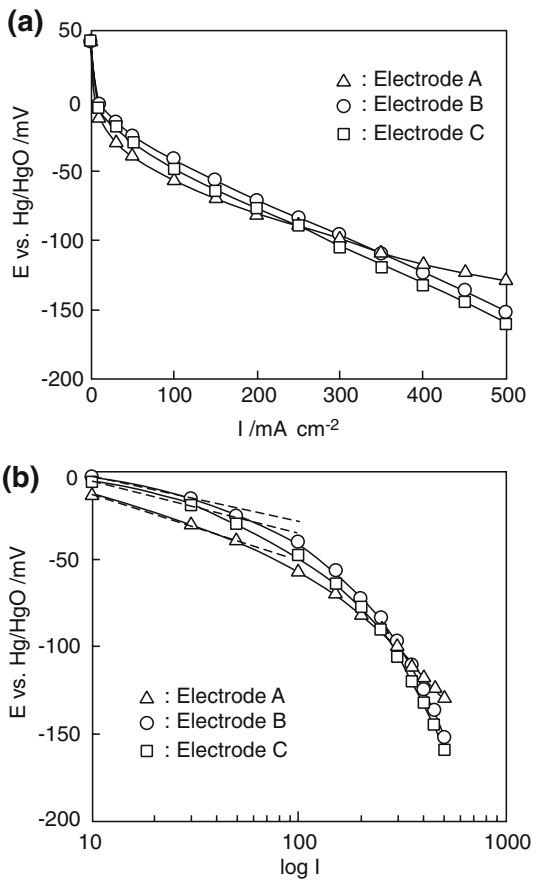

Fig. 3 Polarization curves of conventional-type GDEs with different thicknesses of the $LaMnO_3$/KB catalyst layer (Electrodes A, B, and C). **a** E–I plot, (**b**) Tafel plot (E-logI)

3.2 Effect of electrode structure on oxygen reduction properties

The oxygen reduction activity of three-layer-structured GDEs with two catalyst layers was then investigated. As mentioned above, for thick GDEs, it is important to optimize the structure of the catalyst layer to promote the oxygen diffusion. Therefore, we inserted another catalyst layer, composed of $LaMnO_3$/VX, with a lower surface area between the $LaMnO_3$/KB catalyst layer and the gas diffusion layer, as shown in Fig. 1b. It was expected that the lower surface area of VX would result in a looser packing density and thus improve the gas diffusion. The fabricated electrode is referred to as Electrode D. The polarization curve of Electrode D is shown in Fig. 4, together with that of Electrode A with the single $LaMnO_3$/KB catalyst layer. Electrode D exhibited smaller overpotentials than Electrode A, over the examined current range, despite the increase in the thickness of the GDEs. In addition, the abrupt decrease in potential at higher current densities was also reduced. In order to confirm the above enhancement in the electrode performance, the stacking order of the $LaMnO_3$/VX and $LaMnO_3$/KB layers was switched, i.e., the $LaMnO_3$/VX layer was formed on the electrolyte side. This electrode is referred to as Electrode E, and the polarization curve is also shown in Fig. 4. In contrast, the oxygen reduction activity of Electrode E decreased, compared to that of Electrode D. In order to account for such a trend, the pore size distribution, surface area, and gas permeability of the $LaMnO_3$/KB and $LaMnO_3$/VX layers were subsequently examined. Figure 5 shows the pore size distribution of the gas diffusion layer and the $LaMnO_3$/KB, and $LaMnO_3$/VX catalyst layers, measured using a mercury porosimeter. The pore sizes, at maximum pore volume, for the gas diffusion layer and $LaMnO_3$/VX layer were around 90 and 30 nm, respectively. Such submicron sized pores serve as a good pathway for oxygen diffusion. The $LaMnO_3$/KB layer, however, showed a pore size distribution which was broad, and no obvious pore size at maximum pore volume was observed. This suggests the presence of a much lower number of submicron pores, resulting in efficient gas diffusion. This indicates that the $LaMnO_3$/KB layer is more densely packed with particles, due to the high surface area of KB. Table 2 shows the surface area and gas permeability of the $LaMnO_3$/KB and $LaMnO_3$/VX layers, fabricated on nickel meshes. The gas permeability of the $LaMnO_3$/VX layer is much higher than that of the $LaMnO_3$/KB layer. Thus, it can be concluded that the improved gas supply through the $LaMnO_3$/VX layer is responsible for the enhanced performance of Electrode D. Note that for Electrode E, the dense $LaMnO_3$/KB layer possibly hinders the gas diffusion to the $LaMnO_3$/VX layer in contact with the electrolyte. Thus, the

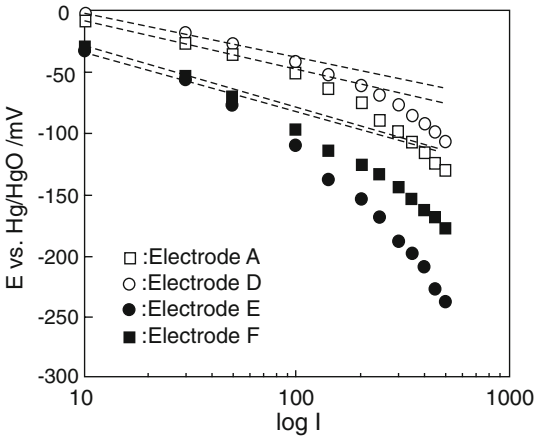

Fig. 4 Tafel plot of polarization for three-layer-structured GDEs (Electrodes D and E with the two $LaMnO_3$/KB and $LaMnO_3$/VX catalyst layers) and conventional-type GDEs (Electrodes A and F with single $LaMnO_3$/KB and $LaMnO_3$/VX catalyst layers, respectively)

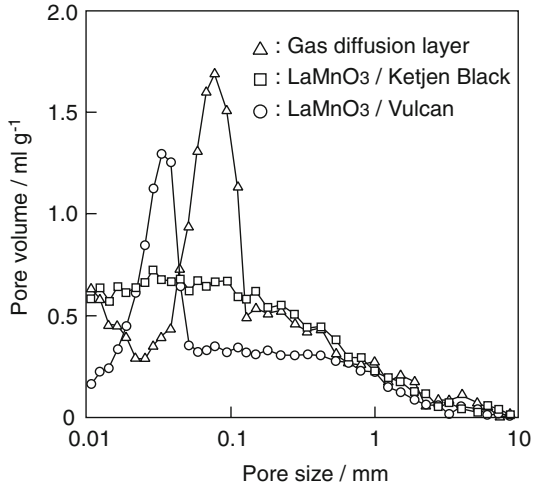

Fig. 5 Pore size distributions of the gas diffusion layer, $LaMnO_3$/KB, and $LaMnO_3$/VX catalyst layers

Table 2 Surface area and gas permeability of the $LaMnO_3$/KB and $LaMnO_3$/VX layers

	$LaMnO_3$/Ketjen Black	$LaMnO_3$/Vulcan XC-72
Surface area ($m^2\ g^{-1}$)	772	115
Gas permeability ($mL\ cm^{-2}cm\ s^{-1}\ atm^{-1}\ cm^{-2}$)	0.085	0.195

consequent shortage in oxygen significantly increased the overpotentials of Electrode E, at high current densities.

In addition to the porosity and gas permeability measurements, the oxygen reduction activity of the $LaMnO_3$/VX layer was also examined. Figure 4 shows the

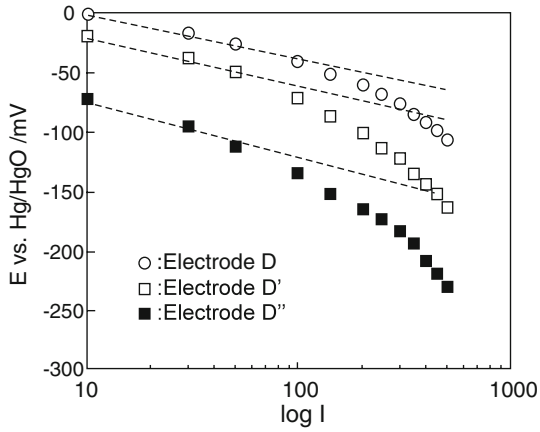

Fig. 6 Tafel plot of polarization for three-layer-structured GDEs with and without the $LaMnO_3$ catalyst (Electrodes D, D′, and D″)

polarization curve of Electrode F with the single $LaMnO_3$/VX catalyst layer. Electrode F shows much larger overpotentials when compared to Electrode A, indicating that $LaMnO_3$/VX has a lower catalytic activity than that of $LaMnO_3$/KB. It is reasonable to postulate that the $LaMnO_3$/VX catalyst layer, with a lower surface area, has a lower number of oxygen reduction sites compared to the $LaMnO_3$/KB layer. Thus, the $LaMnO_3$/KB layer, with the high catalytic activity, should be stacked onto the electrolyte side to effectively reduce oxygen diffusing through the $LaMnO_3$/VX catalyst layer.

In order to more clearly understand the role of the $LaMnO_3$ catalyst, two electrodes without the presence of catalyst, referred to as Electrodes D′ and D″, were fabricated and tested for their oxygen reduction activities. The basic structures of Electrodes D′ and D″ are the same as that of Electrode D. However, the $LaMnO_3$ catalyst was removed from the VX layer of Electrode D and from the KB layer of Electrode D″, as shown in Table 1. The polarization curves of Electrodes D, D′, and D″ are shown in Fig. 6. The overpotentials of Electrodes D′ and D″ were significantly larger than those of Electrode D, indicating that the $LaMnO_3$ catalyst plays a critical role in oxygen reduction. It is noted that the increase in the overpotentials was larger for Electrode D″ than D′. This is consistent with the above results which showed that $LaMnO_3$/VX has a lower catalytic activity than $LaMnO_3$/KB.

Finally, the thickness of the three-layer-structured GDE with the two catalyst layers was further increased from 340 to 540 μm. The fabricated electrode was referred to as Electrode G. Figure 7 shows the polarization curve of Electrode G, together with those of Electrodes B and D. Remarkably, the oxygen reduction activity of the three-layer-structured GDE increased with increasing electrode thickness. This was probably due to an increase in the number of reaction sites, although a slight potential drop

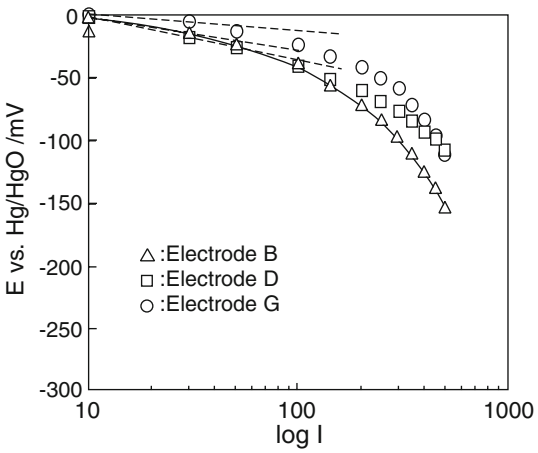

Fig. 7 Tafel plot of polarization for a conventional-type GDE (Electrode B) and three-layer-structured GDEs with different thicknesses (Electrodes D and G)

was observed at high current densities. Furthermore, the electrode potential of Electrode G at the current density 300 mA cm^{-2} was small (−57 mV), when compared to that of Electrode B (which had the conventional electrode structure), even though the thickness of Electrodes G and B was the same. Therefore, the structural optimization of the catalyst layers holds the key to decreasing the overpotential at high current densities, particularly when the catalyst layers are thicker. Further control of the pore structure and thickness of the catalyst layers would make it possible to fabricate thicker GDEs with higher oxygen reduction activities and stabilities.

4 Conclusions

A three-layer-structured GDE with two catalyst layers loaded with $LaMnO_3$ is designed and tested for its oxygen reduction activity in an alkaline solution. The preliminary experiments revealed that the overpotentials for oxygen reduction of the conventional GDEs, having the $LaMnO_3$/KB catalyst and gas diffusion layers, increased by increasing the thickness of the catalyst layer. This was due to the limitation of the oxygen supply to the reaction sites in contact with the electrolyte. In contrast, the newly developed GDEs, in which a more porous $LaMnO_3$/VX catalyst layer was inserted between the $LaMnO_3$/KB catalyst layer and the gas diffusion layer, exhibited smaller overpotentials even when the thickness of the catalyst layer was increased. Such an improvement was thought to be caused by efficient oxygen supply through the $LaMnO_3$/VX layer to the reaction sites. The control experiments proved that the $LaMnO_3$, deposited on the KB and VX, works as an efficient catalyst for oxygen reduction. The results obtained indicate that the oxygen reduction properties of GDEs are governed not only by the number of catalytic reaction sites but also by the gas permeability in the catalyst layer.

Acknowledgment This study was supported by CREST of JST (Japanese Science and Technology Corporation).

References

1. Zaromb S (1962) J Electrochem Soc 109:1125
2. Foller PC (1986) J Appl Electrochem 16:527
3. Morimoto T, Suzuki K, Matsubara T, Yoshida N (2000) Electrochim Acta 45:4257
4. Kiros Y, Pirjamali M, Bursell M (2006) Electrochim Acta 51:3346
5. Bidault F, Brett DJL, Middleton PH, Brandon NP (2009) J Power Sources 187:39
6. Alcaide F, Cabot P-L, Brillas E (2006) J Power Scources 153:47
7. Morrison MM, Roberts JL Jr, Sawyer DT (1979) Inorg Chem 18:1971
8. Yeager E (1984) Electrochim Acta 29:1527
9. Taylor EJ, Anderson EB, Vilambi NRK (1992) J Electrochem Soc 139:L45
10. Mukerjee S, Srinivasan S, Soriaga MP (1992) J Electrochem Soc 142:1409
11. Beard BC, Ross PN Jr (1990) J Electrochem Soc 137:3368
12. Kiros Y (1996) J Electrochem Soc 143:2152
13. Genieas L, Faure R, Durand R (1998) Electrochim Acta 44:1317
14. Watanabe M, Tomikawa M, Motoo S (1985) J Electroanal Chem 182:193
15. Tseung ACC, Wong LL (1972) J Appl Electrochem 2:211
16. Miura N, Gomyo K, Yamazoe N, Seiyama T (1981) Chem Lett 1279
17. Furuya N, Aikawa H (2000) Electrochim Acta 45:4251
18. Jiang SP, Tseung ACC (1990) J Electrochem Soc 137:3442
19. Bagoizky VS, Shumilov NA, Khrushcheva E (1976) Electrochim Acta 21:919
20. Kanungo SB, Parida KM, Sant BR (1981) Electrochim Acta 26:1157
21. Klapste B, Vondrak J, Velicka J (2002) Electrochim Acta 47:2365
22. Yang J, Xu JJ (2003) Electrochem Commun 5:306
23. Burshtein RH, Vilinskaya VS, Tarasevich MR, Bulavina NG (1976) React Kinet Catal Lett 4:159
24. Raj IA, Vase KI (1990) Int J Hydrogen Energy 15:751
25. Meadowcroft DB (1970) Nature 226:847
26. Hyodo T, Hayashi M, Miura N, Yamazoe N (1996) J Electrochem Soc 143:L266
27. Solla-Gullon J, Montiel V, Aldaz A, Clavilier J (2000) J Electroanal Chem 491:69
28. Osseo-Asare K, Arriagada FJ (1990) Colloid Surf 50:321
29. Khiew PS, Radiman S, Huang NM, Md Soot Ahmad (2003) J Cryst Growth 254:235
30. Yuasa M, Sakai G, Shimanoe K, Teraoka Y, Yamazoe N (2004) J Electrochem Soc 151:A1477
31. Yuasa M, Shimanoe K, Teraoka Y, Yamazoe N (2007) Catal Today 126:313
32. Yuasa M, Sakai G, Shimanoe K, Teraoka Y, Yamazoe N (2004) J Electrochem Soc 151:A1690